ORIGINAL ARTICLE

Off-line motion correction methods for multi-frame PET data

**Jurgen E. M. Mourik · Mark Lubberink ·
Floris H. P. van Velden · Adriaan A. Lammertsma ·
Ronald Boellaard**

Abstract

Purpose Patient motion during PET acquisition may affect measured time-activity curves, thereby reducing accuracy of tracer kinetic analyses. The aim of the present study was to evaluate different off-line frame-by-frame methods to correct patient motion, which is of particular interest when no optical motion tracking system is available or when older data sets have to be reanalysed.

Methods Four different motion correction methods were evaluated. In the first method attenuation-corrected frames were realigned with the summed image of the first 3 min. The second method was identical, except that non-attenuation-corrected images were used. In the third and fourth methods non-attenuation-corrected images were realigned with standard and cupped transmission images, respectively. Two simulation studies were performed, based on [11C]flumazenil and (*R*)-[11C]PK11195 data sets, respectively. For both simulation studies different types (rotational, translational) and degrees of motion were added. Simulated PET scans were corrected for motion using all correction methods. The optimal method derived from these simulation studies was used to evaluate two (one with and one without visible movement) clinical data sets of [11C]flumazenil, (*R*)-[11C]PK11195 and [11C]PIB. For these clinical data sets, the volume of distribution (V_T) was derived using Logan analysis and values were compared before and after motion correction.

Results For both [11C]flumazenil and (*R*)-[11C]PK11195 simulation studies, optimal results were obtained when realignment was based on non-attenuation-corrected images. For the clinical data sets motion disappeared visually after motion correction. Regional differences of up to 433% in V_T before and after motion correction were found for scans with visible movement. On the other hand, when no visual motion was present in the original data set, overall differences in V_T before and after motion correction were $<1.5\pm1.3\%$.

Conclusion Frame-by-frame motion correction using non-attenuation-corrected images improves the accuracy of tracer kinetic analysis compared to non-motion-corrected data.

Keywords PET · Motion correction · Kinetic modelling · Volume of distribution

J. E. M. Mourik (✉) · M. Lubberink · F. H. P. van Velden · A. A. Lammertsma · R. Boellaard
Department of Nuclear Medicine & PET Research,
VU University Medical Center,
P.O. Box 7057, 1007 MB Amsterdam, The Netherlands
e-mail: j.mourik@vumc.nl

Introduction

Positron emission tomography (PET) is a medical imaging technique that allows for measurements of tissue function by following the time course of a tracer labelled with a positron emitter. Most dynamic brain scans require an acquisition time of 60–90 min and, for accurate results, the subject should remain in exactly the same position. In practice, however, subject motion is not uncommon, especially not for specific patient groups such as, for example, patients suffering from Alzheimer's or Parkinson's disease.

Full utilisation of improvements in intrinsic spatial resolution of new PET scanners is increasingly hampered by patient motion [1]. Patient motion during a PET scan may reduce effective spatial resolution [2]. More importantly, patient motion may alter measured time-activity

curves (TAC), especially for small regions of interests (ROI), thereby directly affecting the outcome of tracer kinetic analysis.

The simplest method to reduce patient motion during scanning is the use of head restraints. To date, a number of head restraints are available for reducing motion (e.g. [2, 3]). As these head restraints do not eliminate all movements, even more restrictive head restraints exist that fix the skull completely [3]. These restrictive head restraints, however, are very uncomfortable and therefore they are not used frequently. In addition, many patients (e.g. traumatic brain injury, obsessive-compulsive disorder) do not tolerate rigid head fixation.

An alternative is to register motion during scanning using an optical online motion tracking system. Most recent optical motion tracking systems [4–6] enable online correction for motion that occurs within frames (*in-frame* patient motion). Online motion tracking systems have two main advantages. Firstly, when using a motion tracking system, there is no mismatch between emission and transmission scans, as emission data are realigned to the position of the head during the transmission scan. This is very important, because a mismatch between emission and transmission scans leads to erroneous attenuation correction. Secondly, it is possible to correct for in-frame motion, as realignment may take place several times per second. However, motion tracking systems also have some disadvantages. Firstly, older data sets, acquired prior to installation of a motion tracking system, cannot be corrected for patient motion. Secondly, most optical online motion tracking systems require PET data to be acquired in list mode, which is not possible on older PET scanners. Thirdly, online (continuous) motion correction during reconstruction is not trivial and some difficulties with normalisation and attenuation correction still need to be investigated further [7]. Finally, the use of optical (online) tracking systems is not always possible when the view of the patient in the gantry is limited. This is, for example, the case when scanning patients with traumatic brain injury, where the view within the gantry is partly blocked by auxiliary equipment, such as that needed for administering anaesthetics. In those patients, however, motion is observed frequently.

Frame-by-frame motion correction methods correct image data post hoc. Existing frame-by-frame methods use correlation coefficient [8], cross-correlation [9, 10], mutual information [9, 11], standard deviation of the ratio of two images [10, 12], sum of absolute differences [10, 12], mean square difference [10], stochastic sign change [10] or (scaled) least-square difference images [13, 14]. Although, frame-by-frame motion correction methods do not have the same advantages and performance characteristics as online (optical) motion tracking systems [11], they are very useful when no list-mode data are available, when older data have to be reanalysed or when optical tracking is not possible because of a limited view into the PET gantry.

The purpose of this study was to evaluate four different off-line frame-by-frame motion correction methods, previously introduced by Perruchot et al. [9]. Two of these motion correction methods in theory also correct for mismatches between transmission and emission scans. Methods were evaluated extensively using both simulation studies and several clinical data sets, covering both tracers with low and high cerebral uptake.

Materials and methods

Motion correction strategies

This section describes four different motion correction strategies for multi-frame PET data. These methods differ in the way realignment parameters were derived.

Method A: AC-on-AC

The simplest motion correction method is based on the realignment of attenuation-corrected (AC) (standard) PET images. It is assumed that the first x frames of the AC PET scan contain no patient motion and therefore the sum of the first x frames is used as a reference. Frames $x+1...N$, with N being the number of frames, are then realigned to this summed image (Fig. 1a). Using this method, however, mismatches between emission and transmission scans remain.

Method B: NAC-on-NAC

Non-attenuation-corrected (NAC) PET images (Fig. 2b, f) have the advantages, compared to AC PET, that they are less noisy and that the contours near the skull can be better distinguished. In theory, NAC images should provide better realignment than AC images. Again, it is assumed that there is no patient motion during the first x frames, nor between transmission scan and start of emission scan. NAC frames $x+1...N$ are realigned to the sum of the first x NAC frames. Next, the realigned NAC images are forward projected and reconstructed. The result of the reconstruction is a realigned series of AC images. A schematic diagram of method B is shown in Fig. 1b, where a summed (NAC) image of the first x frames is used as reference image.

Method C: NAC-on-μ

A disadvantage of both methods A and B is that they do not correct for a potential mismatch between transmission and emission scans or for movements during the first x frames.
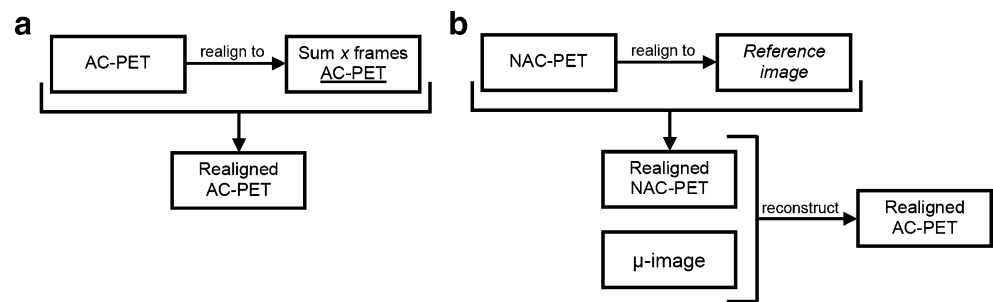
This drawback can be circumvented by using the attenuation map (μ-map or μ-image, Fig. 2c, g), reconstructed from the set of measured attenuation correction factors (ACF), as reference for realignment. All NAC frames are then realigned to the μ-map and reconstructed using the same μ-map for attenuation correction (Fig. 1b, reference image = μ-image).

Method D: NAC-on-cμ

It has been proposed that a variation of the μ-image, the *cupped* μ-image (cμ) [9], is better suited for realigning NAC images, as it has more corresponding contours (Fig. 2d, h).

The cupping effect is obtained as:

$$\mu_{\text{cupped}} = \text{OSEM}\left(\text{ACF}/e^{\text{ACF}}\right)$$

All NAC frames are then realigned to the cupped μ-map and reconstructed using the standard (non-cupped) μ-map for attenuation correction (Fig. 1b, reference image = *cupped* μ-image).

Simulation studies

Simulation studies were used to find optimal settings for the motion correction strategies. Kind of motion, motion correction method and definition of reference image were varied.

Simulated PET scans

Two dynamic PET scans were simulated, each with different tracer uptake. The first had high cortical tracer
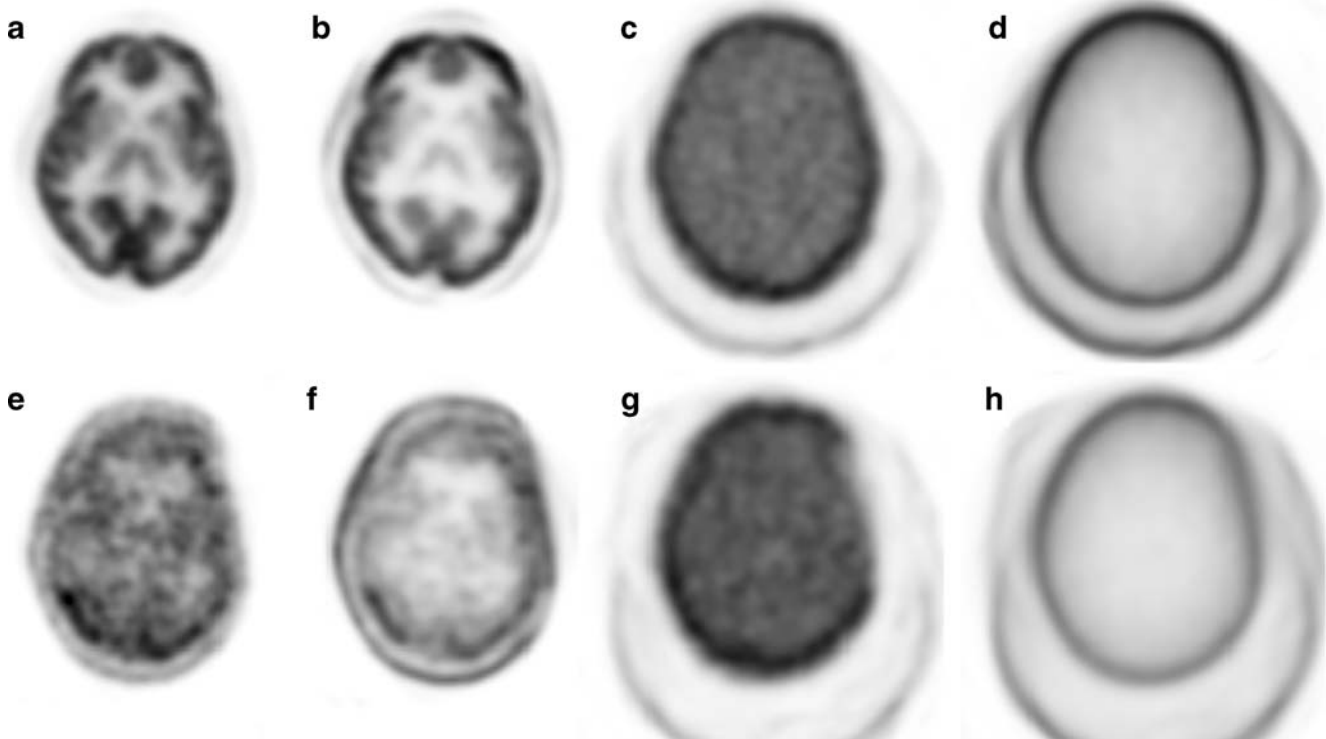

Fig. 2 Examples of a, e attenuation-corrected, b, f non-attenuation-corrected, c, g μ and d, h cupped μ-images for [11C]flumazenil (a–d) and (R)-[11C]PK11195 (e–h) scans

uptake, simulating a tracer like [11C]flumazenil (SIM$_{FMZ}$). In contrast, the second had low tracer uptake, simulating a tracer like (R)-[11C]PK11195 (SIM$_{PK}$). Due to its lower uptake, the latter scan should be more challenging for the motion correction process. Both simulated PET scans were based on a grey-white matter segmented MRI scan. For SIM$_{FMZ}$, a typical [11C]flumazenil grey and white matter TAC was allocated to the grey and white matter segments of the MRI scan, respectively. SIM$_{PK}$ was generated in the same way using typical (R)-[11C]PK11195 grey and white matter TAC. Simulation scans were noise free and smoothed with a Gaussian kernel of ~8 mm full-width at half-maximum (FWHM) to obtain a spatial resolution comparable to that of regular PET images. SIM$_{FMZ}$ and SIM$_{PK}$ consisted of 16 and 23 time frames, respectively, identical to the in-house protocols for clinical studies using these tracers.

Simulated motion

Two types of motion were added to both simulated PET scans. First, different rotations (3, 4, 5 and 6°, Fig. 3, top row) were applied, simulating the 'napping effect' at the end of a scan. These rotational movements correspond to movements of maximum 6.8, 8.2, 9.6 and 11 mm, respectively. The second type of motion simulated axial movements (2, 4, 6, 10 and 20 mm, Fig. 3, bottom row) of a subject. This movement is seen most frequently in clinical practice when subjects are fixed using a head holder. Motion was added using Vinci software (Max Planck Institute for Neurological Research, Cologne, Germany, http://www.mpifnf.de/vinci/). Both rotations and translations were simulated as gradual motions towards the end of the scans, reaching maximum movements in the final frames.

To assess the effect of motion correction when no motion is present, an additional simulation study was performed. This simulation study consisted of 100 motion-free [11C]flumazenil dynamic PET scans. Random noise (~ 8% per pixel) was added to all simulated PET scans to determine the effect of applying motion correction on motion-free data on accuracy and precision of V$_T$.

Motion correction

Automated Image Registration (AIR, version 5.1.5; [15]) was used to realign the simulated PET images. For the present simulation, the 3-D rigid body model using six parameters was used. Prior to the motion correction simulation all (original) images were generated with a clinically relevant spatial resolution of about 8 mm FWHM, as mentioned before. Both the reference image and the images to be aligned were additionally smoothed with a Gaussian kernel of 5 mm FWHM to suppress noise and to speed up realignment (default AIR settings for moderately noisy images). This additional smoothing was applied during the realignment process only in order to obtain the realignment matrix. The realignment matrix was then applied to the original image data (at the clinical image resolution). Thresholds of reference and to be aligned images were varied. Three different cost functions [16] were used, namely (1) standard deviation of ratio image, (2) least squares and (3) least squares with intensity rescaling (adding an intensity scaling term to the model).

Reference image

A reference image was used for motion correction strategies A and B. These reference images are based on the sum of the first x frames of AC PET (method A) or NAC PET (method B). To find optimal settings for the reference image, x was varied from 3 to 10, corresponding to a
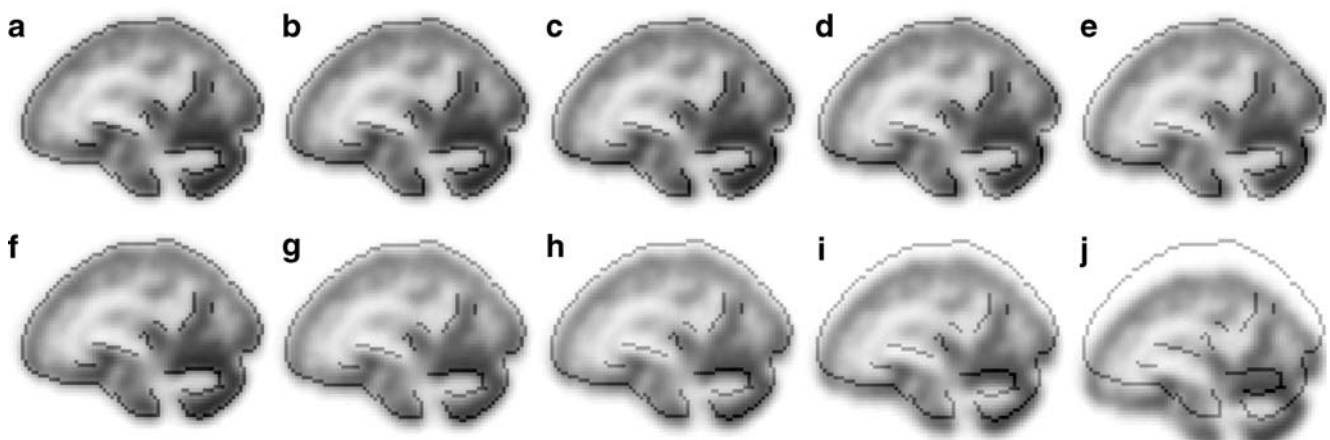

Fig. 3 Different types of motion added to the original simulated [11C] flumazenil PET images (**a**). The *top row* (**b**–**e**) shows rotational movements of 3, 4, 5 and 6°, respectively, and the *lower row* (**f**–**j**) axial translational movements of 2, 4, 6 10 and 20 mm, respectively. The *light grey contour* on top of each image corresponds to the original image (**a**)

summation of the first 45 s to 10 min for SIM_{FLU} and of the first 30 s to 5 min for SIM_{PK}.

Clinical data

Clinical $[^{11}C]$flumazenil, (R)-$[^{11}C]$PK11195 and $[^{11}C]$PIB data were used to assess the simulation results in practice. For all tracers, one subject with large (> 10 mm) and one with no or minor (< 3 mm) movement were selected. For all subjects, the maximal amount of, location of and direction of motion were determined using Vinci software and can be found in Table 1. $[^{11}C]$flumazenil and (R)-$[^{11}C]$PK11195 data were corrected for motion using the optimal setting for SIM_{FMZ} and SIM_{PK}, respectively. $[^{11}C]$PIB data were added as an additional data set to further assess the robustness of the motion correction method. As $[^{11}C]$PIB is a cortical tracer similar to $[^{11}C]$flumazenil, it was corrected for motion using the optimal settings found for SIM_{FMZ}.

All data were taken from clinical study protocols that had been approved by the Medical Ethics Review Committee of the VU University Medical Center. All subjects had given their informed consent prior to scanning.

All scans were acquired using an ECAT EXACT HR+ scanner (CTI/Siemens, Knoxville, TN, USA). Before tracer administration, a 10-min transmission scan was acquired in 2-D mode using rotating $^{68}Ge/^{68}Ga$ sources. This transmission scan was used to correct the subsequent emission scan for attenuation. Subsequently, a dynamic emission scan was acquired in 3-D acquisition mode following bolus injection. Scan duration and frame definition differed per tracer, as described previously [17, 18]. During the emission scan the arterial input function was measured using a continuous flow-through blood sampling device [19]. At set times [17, 18], continuous withdrawal was interrupted briefly for collection of manual samples and, after each sample, the arterial line was flushed with heparinised saline. These manual samples were used for calibrating the (online) blood sampler, for measuring plasma/whole blood ratios and for determining plasma metabolite fractions.

Axial, coronal and sagittal movies were generated for all scans (e.g. see supplementary movies S1 and S2). Each frame of the movie contained a snapshot of the mid-plane of the PET frame, resulting in a movie of N frames. These movies were used to visualise patient motion between frames. To assist visualisation of movements, the edge of

the reference image was projected onto all frames of the movie (e.g. light grey line in Fig. 3). Note that these movies were only used to qualitatively visualise patient motion and that they were not used within the motion correction methods themselves.

Reconstruction settings

Simulation study

Simulation data were reconstructed using normalisation and attenuation-weighted ordered subsets expectation maximisation (NAW-OSEM) to obtain AC PET images. In addition, to obtain NAC PET images, the simulation data were reconstructed using normalisation-weighted OSEM. After realignment, these images were forward projected and then reconstructed using an attenuation-weighted OSEM algorithm. All reconstructions for the simulation study were performed using 4 iterations and 18 subsets and consisted of 63 planes of 128×128 voxels and a voxel size of $2.57 \times 2.57 \times 2.43$ mm^3, identical to the clinical data sets mentioned below.

Clinical data

All data were normalised and corrected for attenuation, random coincidences, scattered radiation, dead time and decay and reconstructed using NAW-OSEM (2 iterations, 16 subsets), as implemented in the standard ECAT 7.2 software (CTI/Siemens, Knoxville, TN, USA), and afterwards smoothed with a Gaussian kernel of 5 mm resulting in an image resolution of 7 mm FWHM. All reconstructed images consisted of 63 planes of 256×256 voxels of $1.29 \times 1.29 \times 2.43$ mm^3, which were rebinned into 63 planes of 128×128 voxels of $2.57 \times 2.57 \times 2.43$ mm^3. In the realignment process, image reconstruction was based on an identical reconstruction method developed in-house.

Analysis

Simulation study

All simulated data were realigned using the above-mentioned motion correction strategies. ROIs were drawn on corresponding SIM_{FLU} or SIM_{PK} T1-weighted MRI

Table 1 Maximum amount and type of motion for the largest movement (clinical data sets)

Tracer	Maximum amount of motion	Type of motion
$[^{11}C]$flumazenil	~11 mm	Mainly rotational
(R)-$[^{11}C]$PK11195	~21 mm	Mainly translation in z direction
$[^{11}C]$PIB	~33 mm	Rotation + translation in z direction

images over different anatomical regions (frontal lobe, pre-frontal lobe, parietal lobe, thalamus, temporal, occipital, thalamus, pons, cerebellum, caudate and putamen) using DISPLAY software (Montreal Neurological Institute, http://www.bic.mni.mcgill.ca/software/Display/Display.html). ROIs were projected onto all frames of the simulated PET scans and TACs were generated as the time sequences of average ROI values. For all anatomical regions, TACs of realigned simulated PET scans were compared with the original (no motion) simulated PET scans. Optimal settings for the simulation study were determined by finding the best combination (method, cost function, reference image generation, etc.) for which differences between regional activity concentrations after motion correction and the true (simulated) activity concentrations were minimal.

Parametric volume of distribution (V_T) images were calculated for all (corrected) simulated PET scans using Logan analysis [20]. Mean V_T values for the various anatomical regions (see above) were calculated and compared with the corresponding original V_T values.

To determine the effect of motion correction on accuracy and precision of V_T with no actual motion present in the data, 100 motion-free simulated PET scans with added noise were analysed both with and without motion correction. Parametric V_T images and mean V_T values for various anatomical regions (see above) were calculated. In addition, per anatomical region, the coefficient of variation (COV, precision) and bias (accuracy) was calculated. The COV (%) was calculated as the standard deviation divided by the mean times 100%. The bias was calculated as the percentage of change in regional V_T values between motion-free simulated PET scans, which were corrected for motion, and the original motion-free simulated PET scans.

Clinical data

All clinical data were realigned using the optimal settings from the simulation study. The result of each realignment was evaluated visually by generating three movies (axial, coronal and sagittal), as described above. V_T images were calculated for both motion-corrected and uncorrected PET images. Ratio images were generated by dividing the V_T image of the motion-corrected data set by the V_T image of the original (uncorrected) data set. Using the software package DISPLAY, a total of 15 ROIs were drawn manually on individually co-registered T1-weighted MRI images in the same anatomical regions as specified above. MRI scans were co-registered to summed images of the first 3 min of the dynamic PET scans. ROIs were projected onto V_T images and mean regional V_T values of uncorrected and motion-corrected TACs were compared.

Results

Simulations

Effect of motion on TAC

TACs of putamen and parietal cortex for SIM_{FMZ} scans without and with added motion are shown in Fig. 4a and b, respectively. Especially for 20-mm translations, differences in parietal lobe TACs were very large (up to 98%).

Effect of motion on V_T

The effects of motion on V_T values for different anatomical regions are shown in Fig. 5. Addition of motion to SIM_{FMZ} (Fig. 5, black symbols) resulted in lower V_T values for all regions (up to −45.6%), except for pons (maximal +13.1%). For SIM_{PK} (Fig. 5, orange symbols), higher V_T values were found for pre-frontal regions (maximal +20.8%) and lower V_T values for all other regions (maximal −45.3%).

Parametric V_T images of SIM_{FMZ} without and with 20-mm translation are shown in Fig. 6a and b, respectively. It
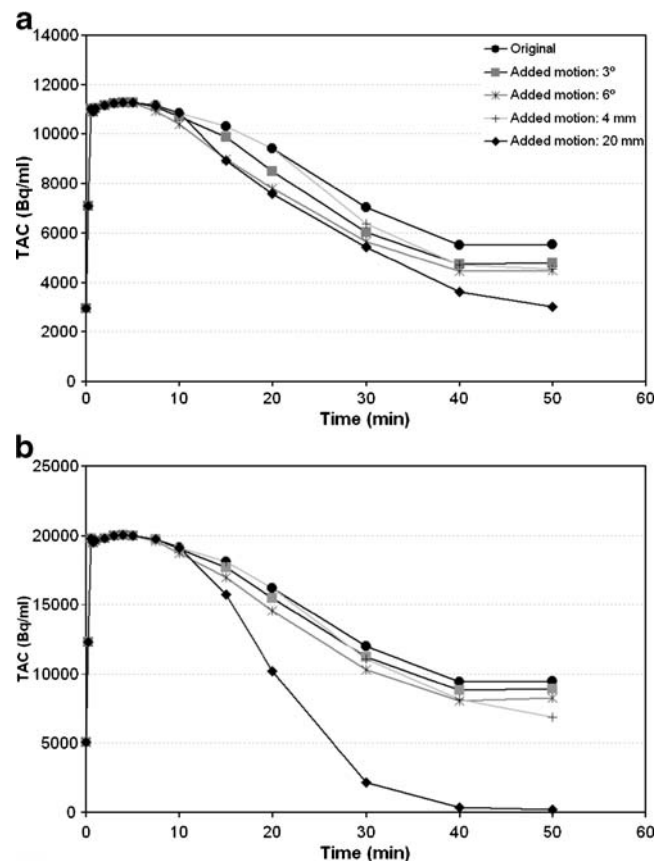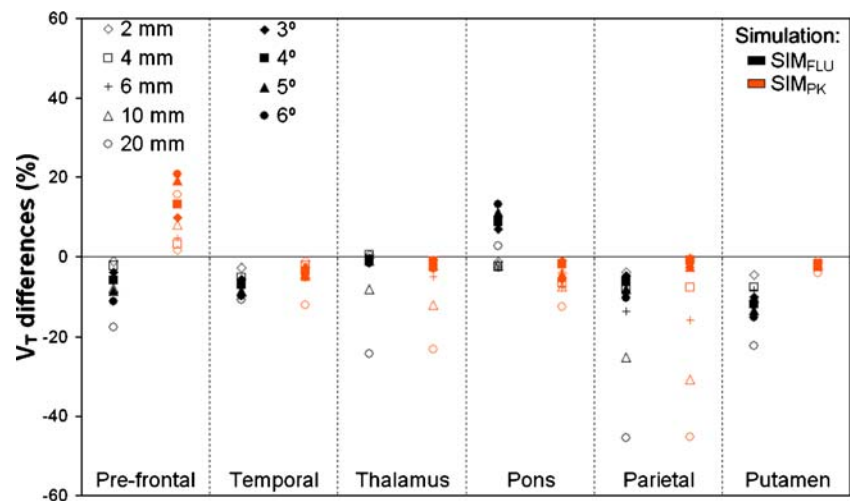

Fig. 4 TACs of **a** putamen and **b** parietal cortex for SIM_{FMZ} scans without and with various degrees of movement (3 and 6° rotation, 4 and 20 mm translation)

can be seen that there are large differences between the two
images. In addition, there are clear artefacts in the image
after translation (Fig. 6b), which are highlighted in the ratio
of both images (Fig. 6d).

Optimal motion correction method

Optimal setting for both SIM_{FMZ} and SIM_{PK} are listed in
Table 2. Figure 7a and b show differences between V_T
values before and after motion correction for SIM_{FMZ} and
SIM_{PK}, respectively, using the optimal combination of
settings found in the simulation study (cost function,
number of summed frames and thresholds) for each
motion correction strategy. For both simulation studies,

best results were obtained using motion correction
strategy B (NAC-on-NAC). Using this method, for
SIM_{FMZ}, maximal differences in V_T values (Fig. 7a, red
symbols) were found for pons (< 2.7%) and putamen
(< 2.8%). For SIM_{PK}, the largest differences in V_T values
(Fig. 7b, red symbols) were found for pre-frontal cortex
(< 3.3%) and pons (< 3.5%). When no motion was added,
no significant differences ($p > 0.20$) were found between
SIM_{FMZ} before and after motion correction, and minimal
effects on accuracy and precision of V_T were found
(Table 3). For SIM_{PK} slightly lower (pons: −3.4%) V_T
values were found after motion correction, but these
values were not significantly different from the original
ones ($p > 0.22$).

Fig. 6 Parametric V_T images of
simulation study. **a** V_T of origi-
nal (no motion) SIM_{FMZ}. **b** V_T
of SIM_{FMZ} after adding 20-mm
translation. **c** As **b** but *after
motion correction*. **d** Ratio im-
age of **a** and **b**. **e** Ratio image of
a and **c**. Note that the range of
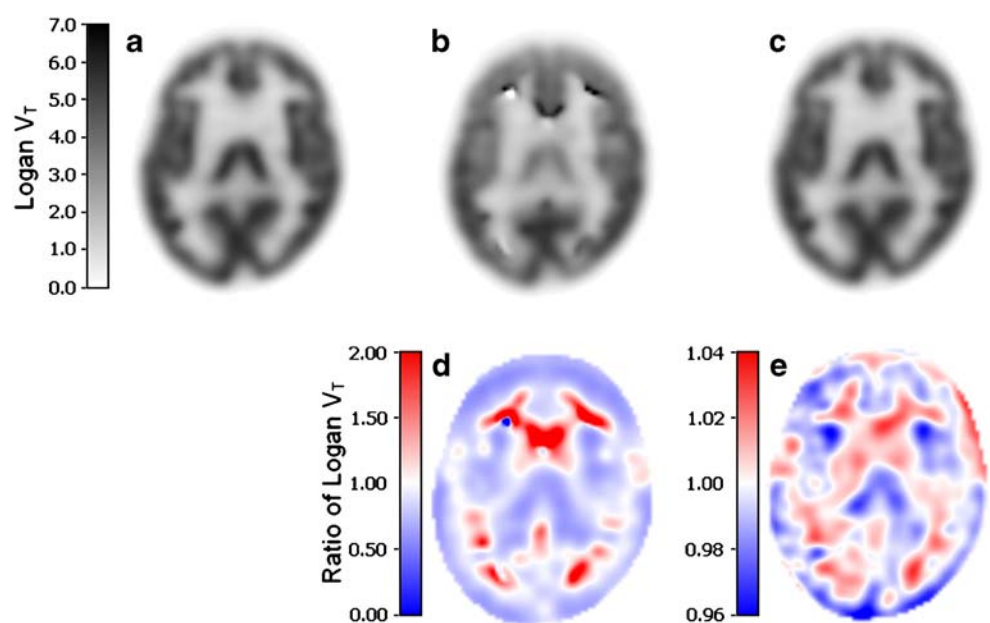the colour scale of **d** and **e** is
different

Table 2 Optimal settings for both simulation studies

Simulation	Optimal method	Cost function	Threshold of aligned frames	Threshold of reference frame	Sum frames
SIM_{FMZ}	NAC-on-NAC	LS	0% MPV	0% MPV	1–6 (0–3 min)
SIM_{PK}	NAC-on-NAC	LSIR	40% MPV	35% MPV	1–8 (0–3 min)

LS least squares, *LSIR* least squares with intensity rescaling, *% MPV* percentage of maximum pixel value

Figure 6c shows a V_T image after motion correction using the optimal settings. The artefacts, as visible on the motion-affected V_T image (Fig. 6b), have completely disappeared. The ratio image between the original V_T image (Fig. 6a) and the motion-corrected V_T image (Fig. 6c) is shown in Fig. 6e. As can be seen, only small differences between original V_T and motion-corrected V_T image were found.

Clinical data

Large movements

Using frame-by-frame movies, all clinical data were inspected for motion visually (supplementary movies S1 and S2). Using this method, no motion could be detected after application of the motion correction algorithm. Figure 8 shows parametric V_T images before and after motion correction, together with corresponding MRI images, for data sets with large movements. For [^{11}C]flumazenil, no large differences between V_T images before and after motion correction can be detected visually. Nevertheless, the ratio image showed significant differences (Fig. 8, top row, last column). At a regional level, the largest differences between V_T values before and after motion correction were found for the parietal lobe (26.9%). For [^{11}C]flumazenil, the difference between V_T before and after motion correction across all anatomical regions was on average 8.3±8.1%. A sagittal animation of the original [^{11}C]

flumazenil data set and the realigned [^{11}C]flumazenil data set is shown in supplementary movie S1.

For both (R)-[^{11}C]PK11195 (Fig. 8, middle row) and [^{11}C]PIB (Fig. 8, bottom row), major differences were seen between V_T images before and after motion correction with large artefacts in the uncorrected V_T image. The large difference between original and corrected images is also clearly visible in the ratio image of both V_T images (Fig. 8, middle row, last column). For [^{11}C]PIB, differences were even more pronounced (Fig. 8, bottom row). At a regional level quantitative differences were as high as 433% (right thalamus). Across all regions, the average difference was 85±121%. Supplementary movie S2 shows the original [^{11}C]PIB data set and the [^{11}C]PIB data set after motion correction. Quantitative differences for (R)-[^{11}C]PK11195 were smaller, with a maximum of 49% (parietal lobe) and an average (across all anatomical regions) of 14.9±15.1%.

Minor movements

Parametric V_T images before and after motion correction, together with corresponding MRI images, for data sets with no or minor movements are shown in Fig. 9. No visual differences between images before and after motion correction could be seen. However, for [^{11}C]flumazenil (Fig. 9, top row), the ratio image suggests that there was some (small) motion present in the original data set. For [^{11}C]flumazenil, the largest difference at regional level was
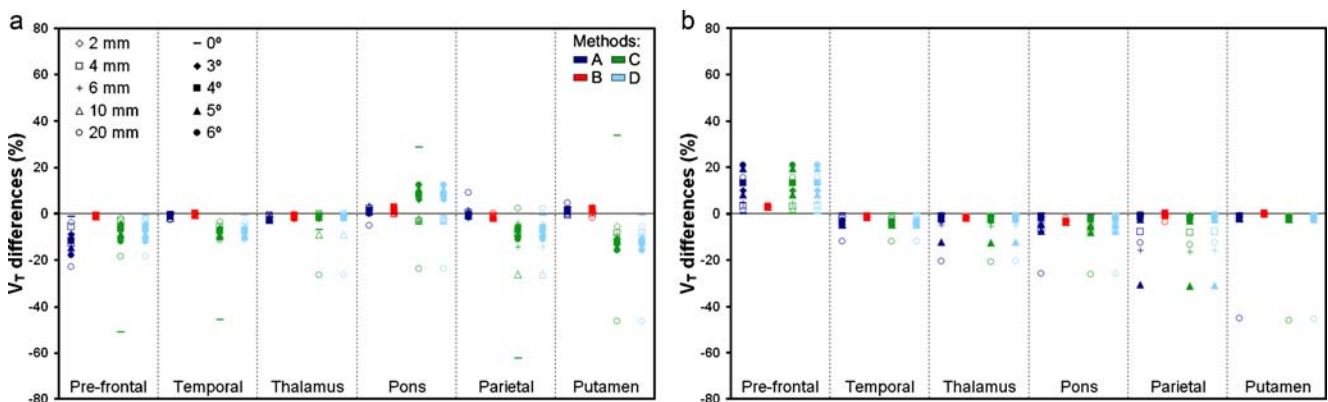

Fig. 7 Differences (%) in V_T between simulated PET scans without and with added motion following motion correction for **a** SIM_{FMZ} and **b** SIM_{PK} using AC-on-AC (*blue symbols*), NAC-on-NAC (*red symbols*), NAC-on-μ realign (*green symbols*) and NAC-on-cμ realign (*light blue symbols*)

Table 3 Precision (COV, %) and bias (accuracy, %) of optimal motion correction method in cases of motion-free simulated PET scans

	COV (%) original	COV (%) after realignment	Bias (%)
Pre-frontal	0.54	0.57	−0.66
Temporal	0.63	1.04	−0.28
Thalamus	1.04	1.11	−0.53
Pons	0.82	1.15	0.80
Parietal lobe	0.47	0.57	0.38
Putamen	1.09	1.39	−0.19

found for right caudate (10.9%), but averaged over all regions differences were only 3.6±3.8%. For both (R)-[^{11}C]PK11195 (Fig. 9, middle row) and [^{11}C]PIB (Fig. 9, bottom row), only small differences were found (max. 4.3%). On average, over all regions, differences between V_T before and after motion correction were 0.4±0.4% and 1.5±1.3% for (R)-[^{11}C]PK11195 and [^{11}C]PIB, respectively.

Discussion

Simulations

The simulation studies showed that motion had a large impact on both regional TACs (max. 98% for the motion parameters selected) and parametric tracer kinetic analysis (max. 45%). Furthermore, these studies showed that the best motion correction method from a theoretical point of view, where emission and transmission scans were aligned (method C or D), did not provide the best results. In fact, for SIM$_{FMZ}$ these methods gave the poorest results (see Fig. 7a, green and light blue symbols) and frequently motion correction failed completely. One reason for these poor results in the case of SIM$_{FMZ}$ may be that the (cupped) μ and PET images (either AC or NAC) only have limited corresponding contours or information (see Fig. 2). Although for SIM$_{PK}$ more corresponding contours or information were seen, motion correction still failed frequently, especially for the last few frames (data not shown).

The best results were obtained for method B, NAC-on-NAC, which is consistent with a previous study performed by Perruchot et al. [9]. This method assumes that there is no motion during the first x minutes. If this assumption holds, and the patient has not moved between transmission and
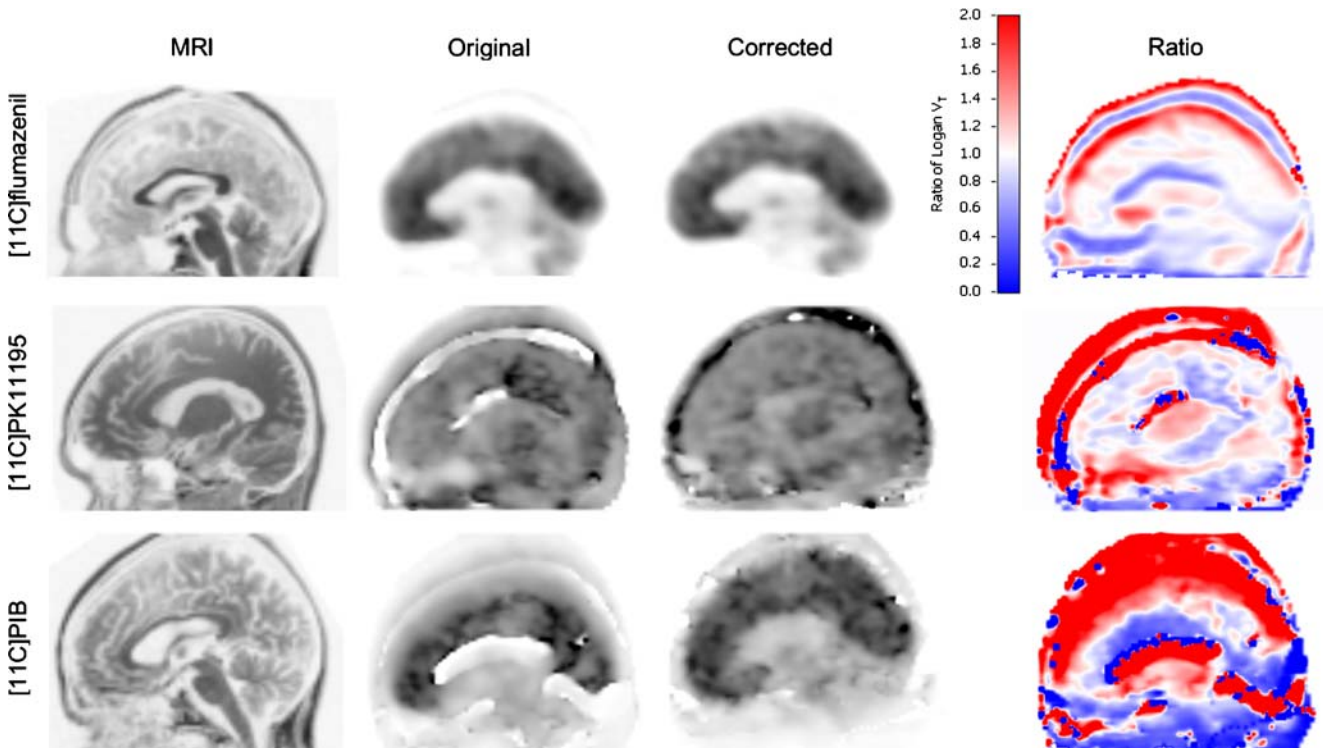

Fig. 8 Differences in V_T images generated from clinical PET scans with *large* movements before and after motion correction. From *left to right*: MRI, parametric V_T images before (original) and after motion correction and ratio image (corrected divided by original) for [^{11}C]flumazenil (*top row*), (R)-[^{11}C]PK11195 (*middle row*) and [^{11}C]PIB (*bottom row*)
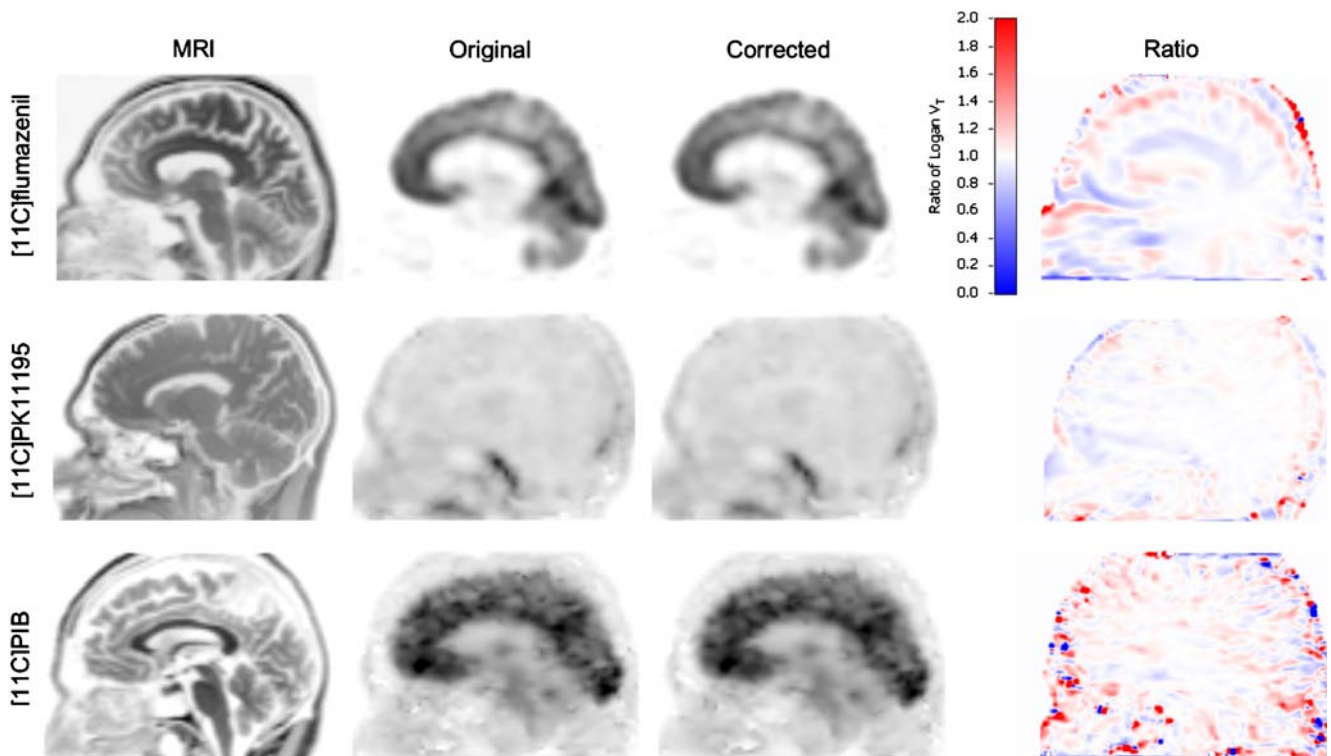
Fig. 9 Differences in V_T images generated from clinical PET scans with *no or minor* movements before and after motion correction. From *left to right*: MRI, parametric V_T images before (original) and after motion correction and ratio image (corrected divided by original) for [11C]flumazenil (*top row*), (R)-[11C]PK11195 (*middle row*) and [11C] PIB (*bottom row*)

emission scan, emission and transmission scans are aligned. Using the optimal motion correction strategy B (NAC-on-NAC), corrected V_T values maximally differed by 3.5% from the original (true) V_T values.

Clinical data

Large movements

Both [11C]flumazenil and (R)-[11C]PK11195 data sets were corrected very well using the settings found in the simulation study. Using frame-by-frame movies and super-imposing the contour of the first x frames is a useful tool to determine whether motion is present.

Differences between original V_T images and V_T images after motion correction were large (up to 49%). In addition, large artefacts, present in the original (R)-[11C]PK11195 V_T images, disappeared when motion correction was applied. Artefacts were less visible in the original [11C]flumazenil V_T images, which is caused by the particular distribution of activity together with the smaller amount of motion in the [11C]flumazenil data set (Table 1). Although visually there was close agreement between V_T images before and after motion correction, both ratio image and ROI analysis showed that the effects of motion were considerable with differences at a regional level being as high as 26.9%.

Therefore, it is recommended that all data be inspected for the presence of motion, e.g. by visual inspection of frame-by-frame movies. In addition, results of the present study indicate that motion correction could always be applied, as effects in case of minor movements are small.

Minor movements

Although the simulation studies already showed that, in the absence of movement, there were no significant changes in V_T values, minor movements were further evaluated for three clinical data sets. Only for the [11C]flumazenil study were small changes in V_T after motion correction observed. This suggests that there was some small movement, although it cannot be excluded that the change was due to the correction algorithm itself. The latter is, however, unlikely as changes for both (R)-[11C]PK11195 and [11C] PIB were very small (max. 1.5±1.3%). These results confirmed those of the simulation studies in that corrections were negligible for minor movements.

Limitations

One limitation of the proposed frame-by-frame motion correction method is its vulnerability to the quality of the scan data and noise characteristics [4]. Montgomery et al.

[11] claimed that problems may occur within the last frame of the PET scan because of poor statistics. This may especially be the case for older data sets acquired on lower sensitivity scanners. In the present study, effects of noise were reduced as much as possible by reconstructing data sets with OSEM, which provides images with less noise then filtered back projection. In addition, images were smoothed (only) during the motion correction process, which was not only helpful for the motion correction optimisation process, but also for reducing the level of noise. Problems with the last frame, as reported by Montgomery et al. [11], were not observed in the present study. Although it is possible that the motion correction algorithm might fail due to low image quality, this does not seem to be likely given the positive results with the low uptake ligand (R)-[^{11}C]PK11195 in the present study.

Another limitation of the frame-by-frame motion correction method is the underlying assumption that there is no significant change in activity distribution within and between frames [4]. This assumption can only be true for the last frames. In fact, the activity distribution varies rapidly in the first frames. For the optimal motion correction method B, the summed reference image has therefore another activity distribution compared to the later frames. However, for the present study, this did not cause any problems during the motion correction process.

The optimal motion correction method derived from the present study assumes that there is no mismatch between the transmission scan and the first x frames of the emission scan. This is a reasonable assumption, because most patient motion appears at later time points of the scan (>10 min) (data not shown). It is, however, recommended that correct alignment of transmission and early (in this case 0–3 min post-injection) emission scans be verified. Nevertheless, if motion appears between transmission and emission scan or within the first 3 min of the emission scan, the mismatch between transmission and emission scans remains. Although motion correction methods C and D correct for emission and transmission mismatch, no satisfactory results were obtained in this study. The use of different cost functions might improve the performance of these methods and therefore have to be investigated. However, for some tracers, like [^{11}C]flumazenil with high cortical uptake, methods C and D will probably always fail because there is too little commonality between the emission (NAC) and μ-images. Even if a mismatch between emission and transmission scans would exist, results of the present study show that a frame-by-frame correction method provides a major improvement in accuracy of pharmacokinetic analyses over non-motion-corrected data.

As mentioned before, the final method derived from the present study does not correct for in-frame motion and therefore motion could still be present within a frame.

However, the present method may be suited to identify suspicious frames and exclude those frames in the following analysis. An easy way to do this is to make a frame-by-frame movie of a data set and identify in which frame the motion starts. Subsequently, the frames before and after the initial motion-affected frame should be visually inspected for any unexpected blurring. A highly blurred frame indicates that there is considerable patient motion during the frame and therefore that frame should be excluded in further analysis.

The AIR package was chosen because it is freely available, easily adjustable and fast. However, it has the disadvantage that only three different cost functions are available. In some applications other cost functions, such as those based on mutual information, may be more appropriate. In those cases, however, it will be necessary to again determine optimal settings for that specific registration algorithm.

Clinical applicability

The present study shows that it is possible to perform an accurate off-line motion correction for dynamic brain studies. In theory, this method should also be applicable to other organs, provided observed motions are rigid. The latter requirement, however, will limit use of the proposed method for non-brain studies. Even when the method would be applicable, optimal settings for the motion correction algorithm need to be re-evaluated for such an application.

For older data sets, no raw data may be available. The optimal method presented here does not require sinogram or list-mode data, but only reconstructed PET and μ-images. Therefore, this method can also be used for accurate motion correction of older data sets.

In clinical practice, subjects are fixed using a head holder. The movements that are most frequently observed are rotations around the x-axis and axial translations. Therefore, only these kinds of movements were included in the simulation study. Clearly, other types of motion (e.g. rotations around the z-axis) may also occur. It should be noted, however, that these types of motion will also be corrected for using the method presented, as all rotational and translational movements are obtained during the registration process.

Conclusion

If no optical tracking system is available or when older data sets need to be reanalysed, a frame-by-frame motion correction method, based on non-attenuation-corrected images, provides major improvements in accuracy of pharmacokinetic analyses over non-motion-corrected data.

References

1. Mourik JEM, van Velden FHP, Lubberink M, Kloet RW, Berckel BNM, Lammertsma AA, et al. Image derived input functions for dynamic high resolution research tomograph PET brain studies. Neuroimage 2008;43:676–86. doi:10.1016/j.neuroimage.2008.07.035.

2. Green MV, Seidel J, Stein SD, Tedder TE, Kempner KM, Kertzman C, et al. Head movement in normal subjects during simulated PET brain imaging with and without head restraint. J Nucl Med 1994;35:1538–46.

3. Beyer T, Tellmann L, Nickel I, Pietrzyk U. On the use of positioning aids to reduce misregistration in the head and neck in whole-body PET/CT studies. J Nucl Med 2005;46:596–602.

4. Rahmim A. Advanced motion correction methods in PET. Iran J Nucl Med 2005;13:1–17

5. Bloomfield PM, Spinks TJ, Reed J, Schnorr L, Westrip AM, Livieratos L, et al. The design and implementation of a motion correction scheme for neurological PET. Phys Med Biol 2003;48:959–78. doi:10.1088/0031-9155/48/8/301.

6. Goldstein SR, Daube-Witherspoon ME, Green MV, Eidsath A. A head motion measurement system suitable for emission computed tomography. IEEE Trans Med Imaging 1997;16:17–27. doi:10.1109/42.552052.

7. Rahmim A, Rousset OG, Zaidi H. Strategies for motion tracking and correction in PET. PET Clin 2007;2:251–66. doi:10.1016/j.cpet.2007.08.002.

8. Andersson JL. A rapid and accurate method to realign PET scans utilizing image edge information. J Nucl Med 1995;36:657–69.

9. Perruchot F, Reilhac A, Grova C, Evans AC, Dagher A. Motion correction of multi-frame PET data. IEEE Nucl Sci Symp Conf Rec 2004;5:3186–90.

10. Lin KP, Huang SC, Yu DC, Melega W, Barrio JR, Phelps ME. Automated image registration for FDOPA PET studies. Phys Med Biol 1996;41:2775–88. doi:10.1088/0031-9155/41/12/014.

11. Montgomery AJ, Thielemans K, Mehta MA, Turkheimer F, Mustafovic S, Grasby PM. Correction of head movement on PET studies: comparison of methods. J Nucl Med 2006;47:1936–44.

12. Andersson JL. How to obtain high-accuracy image registration: application to movement correction of dynamic positron emission tomography data. Eur J Nucl Med 1998;25:575–86. doi:10.1007/s002590050258.

13. Woods RP, Grafton ST, Holmes CJ, Cherry SR, Mazziotta JC. Automated image registration: I. General methods and intra-subject, intramodality validation. J Comput Assist Tomogr 1998;22:139–52. doi:10.1097/00004728-199801000-00027.

14. Woods RP, Grafton ST, Watson JD, Sicotte NL, Mazziotta JC. Automated image registration: II. Intersubject validation of linear and nonlinear models. J Comput Assist Tomogr 1998;22:153–65. doi:10.1097/00004728-199801000-00028.

15. Woods RP, Cherry SR, Mazziotta JC. Rapid automated algorithm for aligning and reslicing PET images. J Comput Assist Tomogr 1992;16:620–33. doi:10.1097/00004728-199207000-00024.

16. Zamburlini M, Camborde M, de la Fuente-Fernandez R, Stoessl AJ, Ruth TJ, Sossi V. Impact of the spatial normalization template and realignment procedure on the SPM analysis of [11C] raclopride PET studies. IEEE Trans Nucl Sci 2004;51:205–11. doi:10.1109/TNS.2003.823030.

17. Mourik JEM, Lubberink M, Klumpers UMH, Lammertsma AA, Boellaard R. Partial volume corrected image derived input functions for dynamic brain studies: methodology and validation for [11C]flumazenil. Neuroimage 2008;39:1041–50. doi:10.1016/j.neuroimage.2007.10.022.

18. Mourik JEM, Lubberink M, Schuitemaker A, Tolboom N, van Berckel BN, Lammertsma AA, et al. Image-derived input functions for PET brain studies. Eur J Nucl Med Mol Imaging 2009;36:463–71. doi:10.1007/s00259-008-0986-8.

19. Boellaard R, van Lingen A, van Balen SC, Hoving BG, Lammertsma AA. Characteristics of a new fully programmable blood sampling device for monitoring blood radioactivity during PET. Eur J Nucl Med 2001;28:81–9. doi:10.1007/s002590000405.

20. Logan J. Graphical analysis of PET data applied to reversible and irreversible tracers. Nucl Med Biol 2000;27:661–70. doi:10.1016/S0969-8051(00)00137-2.